Batteries & Supercaps

Research Article
doi.org/10.1002/batt.202300504

Chemistry Europe
European Chemical Societies Publishing

www.batteries-supercaps.org

VIP *Very Important Paper*

Special Collection

Developing a Hydrophobic Mixed Conductive Interlayer for High-Performance Solid-State Lithium Batteries

Jin Wang,[a] Jiang-Wei Chu,[a, b] Zi-Wei Li,[c] Yu-Long Liang,[c] Tong Liu,[a, b] Jian-Wei Liu,[a, b] Gang Huang,*[a, b] and Xin-Bo Zhang*[a, b]

Garnet solid-state electrolytes (SSEs) $Li_{6.5}La_3Zr_{1.5}Ta_{0.5}O_{12}$ (LLZTO) suffer from poor air stability, producing Li_2CO_3 by-products and causing poor interfacial contact against the Li metal. Obtaining hydrophobic and lithiophilic surface of LLZTO is meaningful for high-performance solid-state batteries. Here, a hydrophobic CF_x film is firstly introduced on the LLZTO surface (CF_x-LLZTO) by magnetron sputtering the polytetrafluoroethylene (PTFE) target. Benefit from its outstanding hydrophobicity, this CF_x film provides the LLZTO a Li_2CO_3-free surface. Moreover, the LiC-LiF mixed conductive interlayer is formed through the reaction between CF_x film and Li metal, resulting in a low interfacial resistance of 73.49 Ω/cm^2. In addition, the LiC-LiF mixed conductive interlayer can also homogenize the electric-field distribution and enable fast Li^+ conduction. As a result, the construction of the hydrophobic mixed conductive interlayer makes the CF_x-LLZTO based symmetric Li/Li cell exhibit a high critical current density of 1.2 mA/cm^2 and a stable cycling life for over 1200 h at 0.1 mA/cm^2. Furthermore, the Li/$LiFePO_4$ cells with the CF_x-LLZTO show improved cycling and rate performance at room temperature. This work provides a practical solution for achieving high-performance solid-state lithium batteries.

Introduction

Garnet solid-state electrolytes (SSEs), represented by $Li_{6.5}La_3Zr_{1.5}Ta_{0.5}O_{12}$ (LLZTO), are potential electrolytes for achieving high-performance solid-state batteries due to its good stability with Li metal, wide electrochemical window and high ionic conductivity.[1] However, the development of LLZTO-based solid-state batteries is hampered by poor interfacial contact and serious Li dendrite.[2] The poor Li metal/LLZTO interfacial contact is imputed to uncontrollable Li_2CO_3 production on LLZTO surface upon moisture exposure, which obstructs the wetting of LLZTO by Li metal, further inducing dendrites formation.[3] As a result, LLZTO usually shows limited critical current density (CCD). Furthermore, LLZTO-based Li metal solid-state batteries also exhibit unsatisfactory cycle life and rate performance.[4]

There are several approaches suggested to address the interface issue, including the introduction of an interlayer, the use of Li alloy, the removal of Li_2CO_3, and the dropping of organic electrolyte.[5] The most common method among these is to introduce interlayer.[6] The earliest commonly utilized interlayers are alloys. Many substances that could be alloyed with Li metal have been used, including Au, Mg, Ag, C, and Sb.[7] These alloy interlayers effectively improved interfacial contact between Li metal and LLZTO. But, these alloy interlayers underwent severe volume change, accompanied with the loss of good contact between Li metal and LLZTO, causing the deterioration of battery performance. Ionic conductive interlayers were then proposed to overcome the disadvantages of alloy interlayers. Li_3PO_4, MoS_2, $LiBH_4$ and polymer SSEs were tentatively employed and improved the batteries performance to some extent.[8] Unfortunately, Li metal solid-state batteries with these ionic conductive interlayers have to operate at high temperature due to their poor room-temperature ionic conductivity. Recently, mixed ionic/electron conductive interlayers have been investigated, such as Li_3N/Cu and Li_2S/LiSn.[9] Mixed conductive interlayers significantly enhance the performance of the LMSSBs by supplying fast ion/electron transport channels as well as limiting alloy volume expansion. However, these mixed ionic/electron conductive interlayers can not prevent the formation of Li_2CO_3 on the surface of LLZTO because they are unable to inhibit moisture from accessing to the LLZTO. Therefore, it is meaningful but challenging to design a hydrophobic mixed ionic/electron conductive interlayer.

In this work, a CF_x film with the feature of outstanding hydrophobicity is firstly introduced on the LLZTO surface by magnetron sputtering the polytetrafluoroethylene (PTFE) target. Benefiting from its outstanding hydrophobicity, this CF_x film

[a] Dr. J. Wang, J.-W. Chu, Prof. T. Liu, Prof. J.-W. Liu, Prof. G. Huang, Prof. X.-B. Zhang
State Key Laboratory of Rare Earth Resource Utilization
Changchun Institute of Applied Chemistry
Chinese Academy of Sciences
Changchun, 130022 (China)
E-mail: ghuang@ciac.ac.cn
xbzhang@ciac.ac.cn

[b] J.-W. Chu, Prof. T. Liu, Prof. J.-W. Liu, Prof. G. Huang, Prof. X.-B. Zhang
School of Applied Chemistry and Engineering
University of Science and Technology of China
Hefei, 230026, China

[c] Z.-W. Li, Y.-L. Liang
Key Laboratory of Automobile Materials
Ministry of Education and College of Materials Science and Engineering
Jilin University
Changchun, 130022 (China)

Supporting information for this article is available on the WWW under https://doi.org/10.1002/batt.202300504

Special Collection An invited contribution to a Special Collection on Young Scientists in Battery Research

Research Article
doi.org/10.1002/batt.202300504
Chemistry Europe
European Chemical Societies Publishing

ensures the LLZTO a Li_2CO_3-free surface even after being exposed to air for a week. Moreover, this CF_x film achieves good contact between the LLZTO and Li metal through the conversion reaction between the Li metal and CF_x at 200 °C. The resulted LiC-LiF mixed ionic/electron conductive layer can homogenize the electric-field distribution and enable fast Li^+ conduction. As a proof of concept, the CF_x interface makes the Li/Li and Li/$LiFePO_4$ cells exhibits long-term cycling stability.

Results and Discussion

As shown in Figure 1(a), the CF_x film was prepared on LLZTO pellet by magnetron sputtering PTFE target to obtain CF_x film-coated LLZTO (CF_x-LLZTO). Thanks to the excellent hydrophobicity of the CF_x film, CF_x-LLZTO can not come into contact with water, avoiding the production of Li_2CO_3. In addition, the LiC/LiF interfacial layer generated by the reaction of CF_x film and Li metal can evenly distribute Li^+ and e^-, realizing uniform deposition of Li metal. The LLZTO pellets were prepared by solid-state reaction according to our previous work (Figure S1).[10] These LLZTO pellets were polished to remove Li_2CO_3 contaminants before depositing CF_x film. In order to better observe the morphology of the CF_x film, we deposited the film on the glass (CF_x-glass) under different deposition pressure (deposition time: 0.5 h), and selected the deposition parameters with the fastest deposition speed and the best deposition quality. Figure 1(b) and Figure S2 show the surface and cross-section images of CF_x film with different deposition pressure. It can be seen that the deposition speed of the CF_x film is the fastest when the deposition pressure is 0.5 Pa, which can reach 106 nm/min. Moreover, the CF_x film prepared under this deposition condition is compact and flat. In order to investigate the hydrophobicity of the CF_x films prepared under different conditions, X-ray photoelectron spectroscopy (XPS) test and water contact angle test were performed. The F/C ratio is a characteristic value to measure the hydrophobicity of the film. The higher the F/C ratio, the stronger the hydrophobicity. Figure 1(c) and Figure S3 show the XPS spectra of CF_x films deposited under different pressure. When the deposition pressure is 0.3 Pa, 0.5 Pa and 1 Pa, the F/C ratio is 1.194, 1.157 and 1.007, respectively. Clearly, the F/C ratio increases with the decrease of deposition pressure.[11] In other words, the hydrophobicity of the CF_x film increases with the decrease of deposition pressure. The results of water contact angle tests also confirm it (Figure S4). The water contact angle is 107.93°, 106.79° and 105.04°, when the deposition pressure is 0.3 Pa, 0.5 Pa and 1 Pa, respectively. Therefore, the CF_x films obtained under the three deposition pressures all possess excellent hydrophobicity.[12] Considering hydrophobicity, deposition

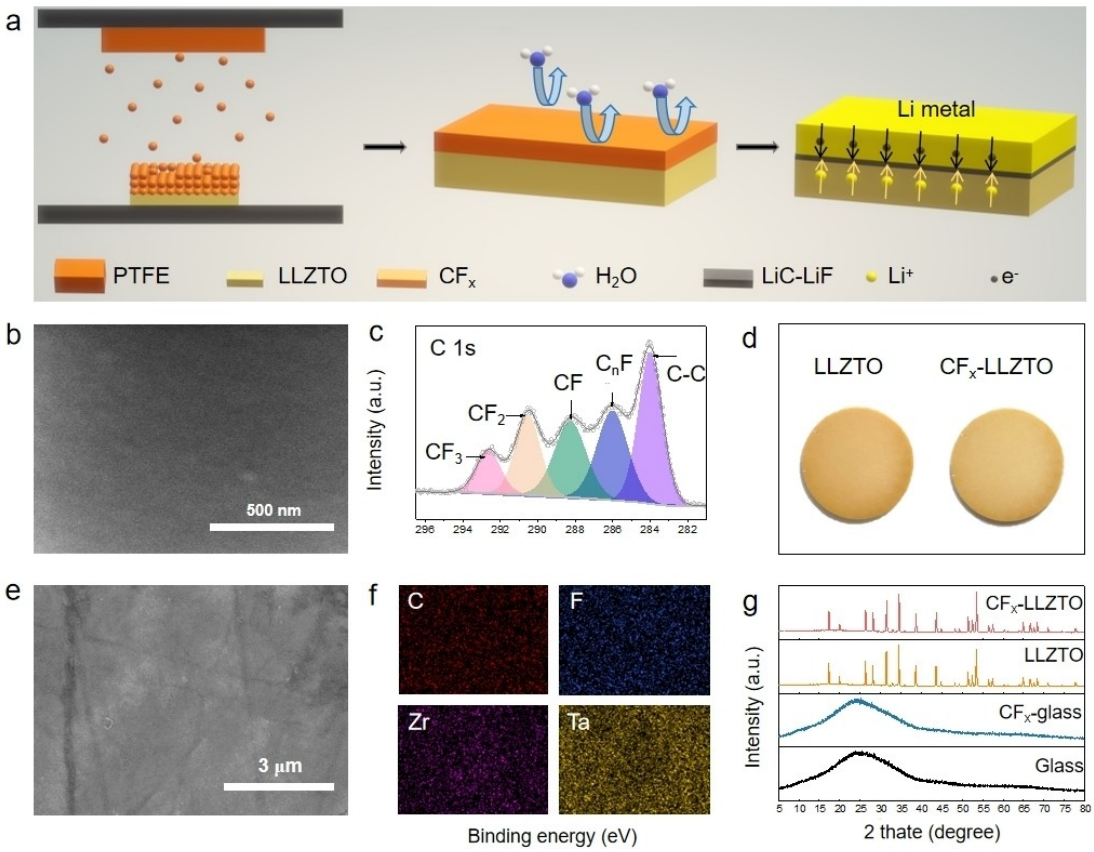

Figure 1. a) Schematic illustration of the preparation of CF_x-LLZTO, the surface stability against air exposure, and the uniform transport of Li^+/e^- in the LiC-LiF interlayer. b) SEM image and c) C 1s XPS spectra of CF_x film. d) Digital pictures of the LLZTO and CF_x-LLZTO. e) SEM image of the CF_x-LLZTO and f) the corresponding energy dispersive spectroscopy (EDS) mapping images of C, F, Zr and Ta elements. g) XRD patterns of the glass, CF_x film coated on glass, LLZTO, and CF_x-LLZTO.

Research Article
doi.org/10.1002/batt.202300504
Chemistry Europe
European Chemical Societies Publishing

speed and deposition quality comprehensively, the deposition pressure was fixed at 0.35 in subsequent experiments.[13] Figure 1(d) shows the digital pictures of pristine LLZTO and CF_x-LLZTO. Because the CF_x film is transparent and colorless (Figure S5), the color of LLZTO does not change before and after magnetron sputtering.[14] Figure 1e and Figure S6 are surface images of the CF_x-LLZTO and LLZTO, respectively. The LLZTO surface exhibits clear polishing scratches. After coating CF_x film, scratches can still be seen on the CF_x-LLZTO, possibly because the film is thin (500 nm), colorless and transparent (Figure S7). In addition, the homogeneous distribution of the C and F elements of CF_x film, and the Zr and Ta elements of LLZTO confirms that the CF_x film did achieve uniform deposition on the LLZTO surface (Figure 1f). X-ray diffraction (XRD) tests were performed to confirm the stability between CF_x and LLZTO. As shown in Figure 1(g), the structure of the CF_x film is amorphous. Besides, the characteristic XRD peaks of the CF_x-LLZTO are almost identical to those of LLZTO, indicating that no undesirable reactions occurred during the magnetron sputtering preparation process.

To check the hydrophobicity of CF_x-LLZTO, water contact angle tests were performed. The surface of LLZTO turns from hydrophilic (water contact angle of 51.93°, Figure 2a) to hydrophobic (water contact angle of 116.05°, Figure 2b) after the CF_x film deposition. Inspired by the successful improvement of the hydrophobicity, its effect on the air stability of the CF_x-LLZTO was investigated. For this purpose, XRD studies of the pellets, following exposure in ambient air for a week, were performed to observe whether CF_x-LLZTO would generate less Li_2CO_3 than LLZTO. As shown in Figure 2(c), Li_2CO_3 was only detected on LLZTO. These results indicate that the CF_x-LLZTO is sufficiently stable against air.[15] These results are encouraging for further studies regarding Li/Li cells and Li/$LiFePO_4$ cells. The quality of interface contact greatly affects the performance of cells, so we compared the morphology of Li/LLZTO interface and Li/CF_x-LLZTO interface. As shown in Figure 2(d), the apparent gap and voids between LLZTO and Li metal indicates the poor wettability of Li metal with LLZTO due to the inevitable Li_2CO_3.[2b] On the contrary, an intimate contact is observed for CF_x-LLZTO (Figure 2e), demonstrating that the interfacial contact was significantly improved by introducing CF_x film. It is necessary to clarify the composition and structure of the interfacial layer formed by reacting CF_x film with molten Li metal. XRD results was shown as Figure 2(f). In addition to the peaks of Li metal, the XRD pattern only shows LiF and LiC corresponding peaks, indicating the conversion reaction of CF_x film to LiF-LiC mixed ionic/electron conductive interlayer was happened. To further clarify the distribution of LiF and LiC, we performed EDS tests on the Li metal/CF_x-LLZTO interface (Figure 2g). From the distribution of F element, it can be seen that LiF exists only at the interface and does not diffuse into the Li metal. It is worth noting that F element also presents inside the LLZTO, which may be due to high temperature will lead to decomposition of CF_x, releasing F_2 gas and then reacting with LLZTO.[16] From the distribution of C element, it can be seen that LiC mainly concentrates at the interface, and a small amount of LiC diffuses into the Li metal. The C element presents in the LLZTO region should be Li_2CO_3 produced by the

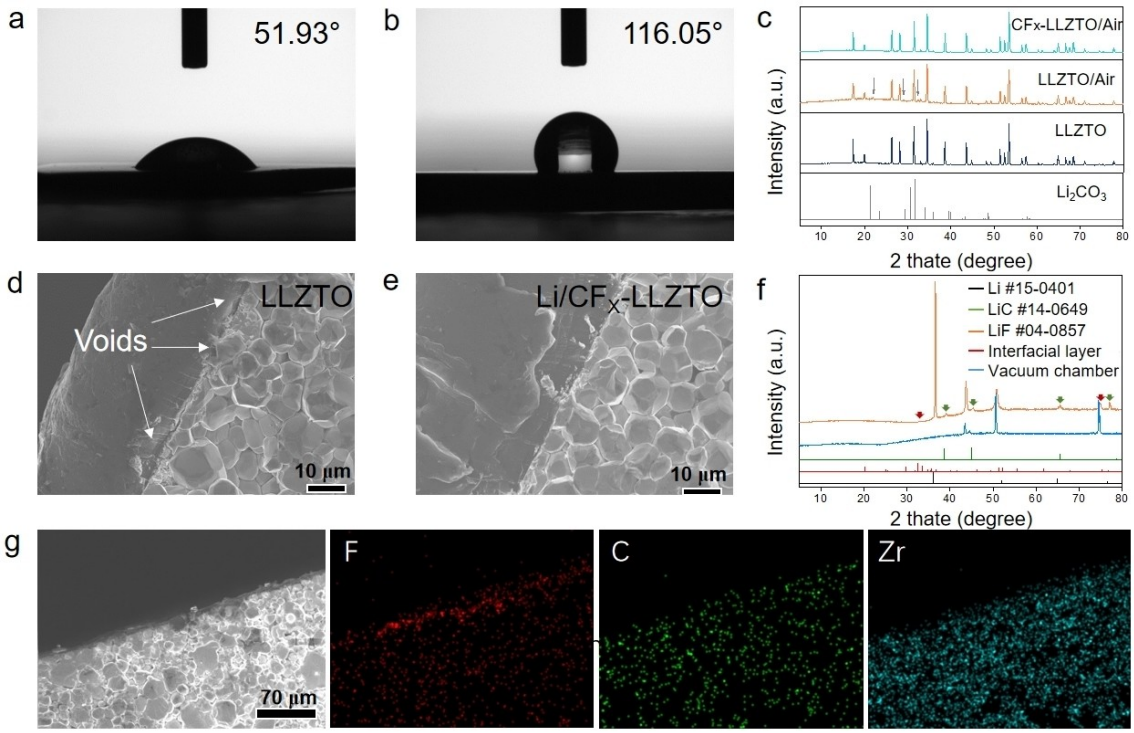

Figure 2. Water contact angle test of the a) LLZTO and b) CF_x-LLZTO. c) XRD patterns of the LLZTO and CF_x-LLZTO before and after air exposure. Cross-section SEM images of the d) Li metal/LLZTO and e) Li metal/CF_x-LLZTO. f) XRD patterns of the reaction products of the Li metal and CF_x film. g) SEM image of the Li metal/CF_x and the corresponding EDS mapping images of F, C and Zr elements.

Research Article
doi.org/10.1002/batt.202300504
Chemistry Europe
European Chemical Societies Publishing

unavoidable exposure of the sample to air during storage and testing.[3a]

Symmetric Li/Li cells were assembled to test the effect of CF_x films on Li metal/LLZTO interface. To quantify the changes of interfacial resistance, electrochemical impedance spectroscopy (EIS) tests was performed (Figure 3a). The Nyquist plots of the Li/Li cell with LLZTO exhibits two semicircles ascribed to the electrolyte resistance and interfacial resistance, respectively.[17] After fitting (Figure S8 and S9), the resistance of Li/LLZTO interface is 270.32 Ω/cm^2. Different from bare LLZTO, the Li/Li symmetric with CF_x-LLZTO exhibits three semicircles which come from the electrolyte resistance, LiF-LiC intermediate layer resistance and LiF-LiC intermediate layer/Li metal interfacial resistance and LiF-LiC intermediate layer/LLZTO interfacial resistance. The total resistance of single Li metal/intermediate layer/LLZTO interfacial resistance is 73.49 Ω/cm^2. This significant decrease in interfacial resistance could be attributed to the improved connection between the LLZTO and the Li metal facilitated by CF_x film. CCD tests were carried out to check the stability of LLZTO/Li interface. As summarized in Figure 3(b), the CCD of Li/Li cell with LLZTO is only 0.3 mA/cm^2. In contrast, the CCD of Li/Li cell with CF_x-LLZTO is enhanced to 1.2 mA/cm^2. This significant improvement of CCD reflects the synergistic advantages of rapid Li^+ transport provided by LiF and uniform electric-field distribution facilitated by LiC. Further, long-term stability of interface was verified by galvanostatic cycling tests. As shown in Figure 3(c), the voltage of the Li/LLZTO/Li battery drops rapidly after only 5 h of cycling, indicating short circuit occurs. The short circuit occurs so quickly because the interface contact is poor, resulting in ultrahigh local current density, which triggers the growth of Li dendrites. To visualize the changes of interface, we disassembled the cells after tests. It is shocked that the Li metal and LLZTO have been completely separated by Li dendrites (Figure 3d). Besides, the cross-section SEM image clearly exhibits the propagation of Li dendrites along LLZTO grains and grain boundaries (Figure S10). In sharp contrast, the Li/Li cell with CF_x-LLZTO shows stable cycles over 1200 h. These results again verified the stable Li metal/CF_x-LLZTO interface. Moreover, no Li dendrites were found either at the interface or inside the CF_x-LLZTO (Figure 3e and Figure S10). However, it needs to be acknowledged that there are ruptures at the Li metal/CF_x-LLZTO interface, which may be due to the volume expansion caused by repeated dissolution-deposition of Li metal. In order to understand the changes of the distribution of LiF-LiC intermediate layer after the cycles, EDS test was performed on the Li metal/CF_x-LLZTO interface. As shown in Figure S11, the content of C element in Li metal is greatly increased and evenly distributed. From the distribution of O element, it can be seen that only the top of Li metal is polluted by the air during the test, so the distribution of C element in Li metal mainly comes from LiC. The distribution of F element has also changed significantly. F element is no longer mainly concentrated at the interface, but is fully and evenly distributed in the Li metal. These phenomena indicate that both LiF and LiC move from the interface to the interior of Li metal as the cycle progresses, which is consistent with the results reported in previous articles.[18]

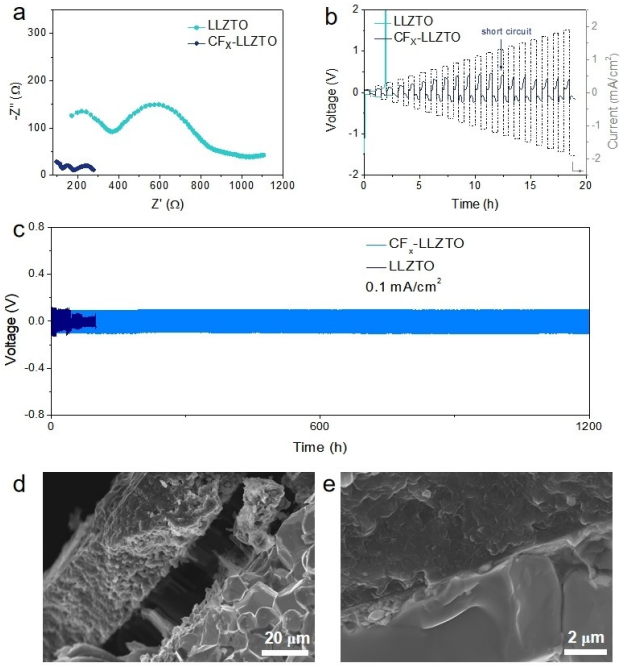

Figure 3. a) EIS, b) CCD, and c) cycle life tests of the symmetric Li/Li cells with LLZTO and CF_x-LLZTO. Cross-section SEM images of d) the Li metal/LLZTO interface and e) Li metal/CF_x-LLZTO interface.

Figure 4(a) shows the rate performance of Li/$LiFePO_4$ cells with LLZTO and CF_x-LLZTO (Figure 4a). The discharge

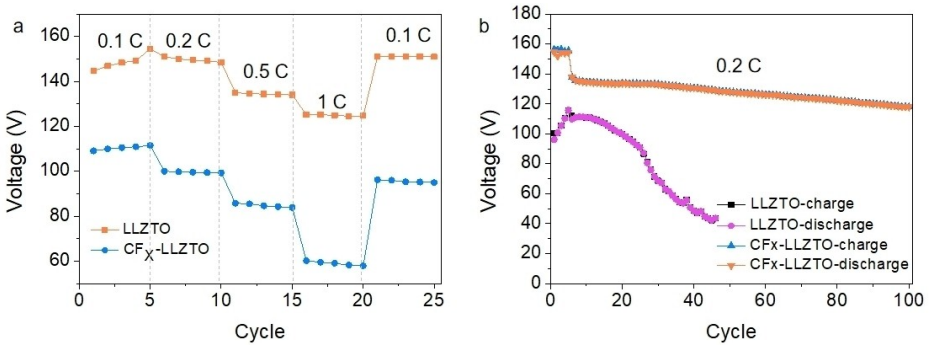

Figure 4. a) Rate performance of the Li/$LiFePO_4$ cells with LLZTO and CF_x-LLZTO. b) Cycle performance of the Li/$LiFePO_4$ cells with LLZTO and CF_x-LLZTO at 0.2 C and room temperature.

capacities of Li/$LiFePO_4$ cells with CF_x-LLZTO are 154.5, 148.5, 134, and 124.7 mAh/g at 0.1 C, 0.2 C, 0.5 C and 1 C, respectively. After high-rate cycling, the discharge capacity recovers to 151 mAh/g at 0.1 C. This outstanding rate performance can be attributed to fast Li^+ conduction, homogenize electric-field distribution and good interface contact. In contrast, the discharge capacities of Li/$LiFePO_4$ cells with LLZTO are 111.5, 99.3, 83.9, and 57.9 mAh/g at 0.1 C, 0.2 C, 0.5 C and 1 C, respectively. In addition, the discharge capacity decreases to 95 mAh/g at 0.1 C after high-rate cycling. Moreover, the Li/$LiFePO_4$ cell with CF_x-LLZTO maintained high capacity retention of 85.5 % after 100 cycles under 0.2 C at room temperature (Figure 4b).

Conclusions

In summary, a novel hydrophobic mixed conductive interlayer at the interface between the Li metal and LLZTO has been designed by magnetron sputtering the PTFE target. The as deposited CF_x film possesses outstanding hydrophobicity, ensuring the LLZTO a Li_2CO_3-free surface. Furthermore, the LiC-LiF mixed conductive interlayer could be formed through the reaction between the CF_x film and Li metal, resulting good interface contact and a low interfacial resistance of 73.49 Ω/cm^2. In addition, the LiC-LiF mixed conductive interlayer can also uniformize the distribution of the electric field and enable fast Li^+ conduction. As a result, the CF_x-LLZTO based Li/Li cell shows a high CCD of 1.2 mA/cm^2 and allows stable cycling for over 1200 h at 0.1 mA/cm^2 without loss of interface contact or formation of Li dendrites. For Li/$LiFePO_4$ full cells with the CF_x-modified LLZTO, they display improved cycling and rate performance at room temperature. This work offers a useful and innovative method for creating hydrophobic mixed conductive interlayers and addressing the interface issues in the solid-state lithium batteries. The proposed approach could also provide valuable insights for enhancing the stability of Li metal, Na metal, and other materials that are sensitive to the air.

Acknowledgements

This work was financially supported by the National Key R&D Program of China (2020YFE0204500), National Natural Science Foundation of China (52171194, 52071311, 52271140), CAS Project for Young Scientists in Basic Research (YSBR-058), Changchun Science and Technology Development Plan Funding Project (21ZY06), Youth Innovation Promotion Association CAS (2020230), Natural Science Foundation of China Excellent Young Scientists (Overseas), and the China Postdoctoral Science Foundation (2022M713070).

Conflict of Interests

The authors declare no conflict of interest.

Data Availability Statement

The data that support the findings of this study are available from the corresponding author upon reasonable request.

Keywords: Li dendrite · hydrophobic · garnet electrolyte · interface · solid-state electrolyte

[1] a) Y. Zhu, M. Chon, C. V. Thompson, J. L. Rupp, *Angew. Chem. Int. Ed.* **2023**, *135*, e202304581; b) C. Wang, K. Fu, S. P. Kammampata, D. W. Mcowen, A. J. Samson, L. Zhang, G. T. Hitz, A. M. Nolan, E. D. Wachsman, Y. Mo, V. Thangadurai, L. Hu, *Chem. Rev.* **2020**, *120*, 4257–4300.
[2] a) A. C. Thenuwara, E. L. Thompson, T. F. Malkowski, K. D. Parrotte, K. E. Lostracco, S. Narayan, R. T. Rooney, L. A. Seeley, M. R. Borges, B. D. Conway, *ACS Energy Lett.* **2023**, *8*, 4016–4023; b) Z. Bi, R. Shi, X. Liu, K. Liu, M. Jia, X. Guo, *Adv. Funct. Mater.* **2023**, *33*, 2307701.
[3] a) H. Huo, J. Luo, V. Thangadurai, X. Guo, C. Nan, X. Sun, *ACS Energy Lett.* **2019**, *5*, 252–262; b) L. Zhang, H. Guo, Q. Zhang, A. Wang, Y. Su, Y. Chen, Y. Li, F. Shen, X. Han, *Energy.* **2023**, *37*, 14341–14349.
[4] a) B.-Q. Xiong, Q. Nian, X. Zhao, Y. Chen, Y. Li, J. Jiang, S. Jiao, X. Zhan, X. Ren, *ACS Energy Lett.* **2022**, *8*, 537–544; b) S. Pazhaniswamy, S. A. Joshi, H. Hou, A. K. Parameswaran, S. Agarwal, *Adv. Energy Mater.* **2023**, *13*, 2202981.
[5] a) T. Wang, J. Duan, B. Zhang, W. Luo, X. Ji, H. Xu, Y. Huang, L. Huang, Z. Song, J. Wen, *Energy Environ. Sci.* **2022**, *15*, 1325–1333; b) X. Feng, H. Fang, N. Wu, P. Liu, P. Jena, J. Nanda, D. Mitlin, *Joule.* **2022**, *6*, 543–587; c) S. Kim, J.-S. Kim, L. Miara, Y. Wang, S.-K. Jung, S. Y. Park, Z. Song, H. Kim, M. Badding, J. Chang, *Nat. Commun.* **2022**, *13*, 1883.
[6] H. Huo, J. Gao, N. Zhao, D. Zhang, N. G. Holmes, X. Li, Y. Sun, J. Fu, R. Li, X. Guo, *Nat. Commun.* **2021**, *12*, 176.
[7] a) R. Dubey, J. Sastre, C. Cancellieri, F. Okur, A. Forster, L. Pompizii, A. Priebe, Y. E. Romanyuk, L. P. Jeurgens, M. V. Kovalenko, *Adv. Energy Mater.* **2021**, *11*, 2102086; b) W. Feng, X. Dong, P. Li, Y. Wang, Y. Xia, *J. Power Sources.* **2019**, *419*, 91–98; c) S. Kim, C. Jung, H. Kim, K. E. Thomas-Alyea, G. Yoon, B. Kim, M. E. Badding, Z. Song, J. Chang, J. Kim, D. Im, K. Kang, *Adv. Energy Mater.* **2020**, *10*, 1903993; d) H. Koshikawa, S. Matsuda, K. Kamiya, M. Miyayama, Y. Kubo, K. Uosaki, K. Hashimoto, S. Nakanishi, *J. Electroanal. Chem.* **2019**, *835*, 143–149; e) Y. Shao, H. Wang, Z. Gong, D. Wang, B. Zheng, J. Zhu, Y. Lu, Y.-S. Hu, X. Guo, H. Li, X. Huang, Y. Yang, C.-W. Nan, L. Chen, *ACS Energy Lett.* **2018**, *3*, 1212–1218.
[8] a) Y. Gao, S. Sun, X. Zhang, Y. Liu, J. Hu, Z. Huang, M. Gao, H. Pan, *Adv. Funct. Mater.* **2021**, *31*, 2009692; b) J. Fu, P. Yu, N. Zhang, G. Ren, S. Zheng, W. Huang, X. Long, H. Li, X. Liu, *Energy Environ. Sci.* **2019**, *12*, 1404–1412; c) J. Liu, X. Gao, G. O. Hartley, G. J. Rees, C. Gong, F. H. Richter, J. Janek, Y. Xia, A. W. Robertson, L. R. Johnson, P. G. Bruce, *Joule.* **2020**, *4*, 101–108; d) H. Huo, Y. Chen, J. Luo, X. Yang, X. Guo, X. Sun, *Adv. Energy Mater.* **2019**, *9*, 1804004.
[9] a) K. Lee, S. Han, J. Lee, S. Lee, J. Kim, Y. Ko, S. Kim, K. Yoon, J.-H. Song, J. H. Noh, *ACS Energy Lett.* **2021**, *7*, 381–389; b) F. Zhu, W. Deng, B. Zhang, H. Wang, L. Xu, H. Liu, Z. Luo, G. Zou, H. Hou, X. Ji, *Nano Energy.* **2023**, *111*, 108416; c) H. Huo, Y. Chen, R. Li, N. Zhao, J. Luo, J. G. P. D. Silva, R. Mücke, P. Kaghazchi, X. Guo, X. Sun, *Energy Environ. Sci.* **2020**, *13*, 127–134.
[10] J. Wang, Y. Yin, T. Liu, X. Yang, Z. Chang, X. Zhang, *Nano Res.* **2018**, *11*, 3434–3441.
[11] J. Kousal, J. Hanuš, A. Choukourov, P. Hlídek, H. Biederman, D. Slavínská, J. Zemek, *Surf. Coat. Technol.* **2005**, *200*, 472–475.
[12] S. Sohn, H.-M. Kim, J. Jang, *J. Korean Phys. Soc.* **2010**, *57*, 1281–1284.
[13] H. Biederman, V. Stelmashuk, I. Kholodkov, A. Choukourov, D. Slavınska, *Surf. Coat. Technol.* **2003**, *174–175*, 27–32.
[14] a) Y.-l. Yu, X.-Q. Xu, T.-H. Zhang, Y. Ma, *Thin Solid Films.* **2020**, *712*, 138302; b) A. Zhuang, K. Wu, Y. Lu, J. Yu, *Micromachines.* **2023**, *14*, 1292.
[15] L. Zhang, H. Guo, Q. Zhang, A. Wang, Y. Su, Y. Chen, Y. Li, F. Shen, X. Han, *Energy Fuels.* **2023**, *37*, 14341–14349.

[16] a) Y. Chen, B. Ouyang, X. Li, W. Liu, B. Yang, P. Ning, Q. Xia, F. Zan, E. Kan, J. Xu, *ACS Appl. Mater. Interfaces.* **2023**, *15*, 44962–44973; b) Y. Yu, G. Huang, J. Z. Wang, K. Li, J. L. Ma, X. B. Zhang, *Adv. Mater.* **2020**, *32*, 2004157.
[17] J. Jiang, Y. Ou, S. Lu, C. Shen, B. Li, X. Liu, Y. Jiang, B. Zhao, J. Zhang, *Energy Storage Mater.* **2022**, *50*, 810–818.
[18] a) H. Duan, W. P. Chen, M. Fan, W. P. Wang, L. Yu, S. J. Tan, X. Chen, Q. Zhang, S. Xin, L. J. Wan, Y. G. Guo, *Angew. Chem. Int. Ed.* **2020**, *59*, 12069–12075; b) Y. G. Lee, S. Fujiki, C. Jung, N. Suzuki, N. Yashiro, R. Omoda, D. Suko, T. Shiratsuchi, T. Sugimoto, S. Ryu, J. H. Ku, T. Watanabe, Y. Park, Y. Aihara, D. Im, I. T. Han, *Nat. Energy.* **2020**, *5*, 299–308.

Manuscript received: October 29, 2023
Revised manuscript received: November 25, 2023
Accepted manuscript online: November 27, 2023
Version of record online: December 14, 2023